



**HAL**  
open science

# Tuning the Photoelectrocatalytic Hydrogen Evolution of Pt-Decorated Silicon Photocathodes by the Temperature and Time of Electroless Pt Deposition

Bruno Fabre, Li Gaozeng, F. Gouttefangeas, L. Joanny, Gabriel Loget

► **To cite this version:**

Bruno Fabre, Li Gaozeng, F. Gouttefangeas, L. Joanny, Gabriel Loget. Tuning the Photoelectrocatalytic Hydrogen Evolution of Pt-Decorated Silicon Photocathodes by the Temperature and Time of Electroless Pt Deposition. *Langmuir*, 2016, 32 (45), pp.11728-11735. 10.1021/acs.langmuir.6b02122 . hal-01416454

**HAL Id: hal-01416454**

**<https://univ-rennes.hal.science/hal-01416454>**

Submitted on 13 Jul 2017

**HAL** is a multi-disciplinary open access archive for the deposit and dissemination of scientific research documents, whether they are published or not. The documents may come from teaching and research institutions in France or abroad, or from public or private research centers.

L'archive ouverte pluridisciplinaire **HAL**, est destinée au dépôt et à la diffusion de documents scientifiques de niveau recherche, publiés ou non, émanant des établissements d'enseignement et de recherche français ou étrangers, des laboratoires publics ou privés.

1  
2  
3  
4  
5  
6  
7  
8  
9  
10  
11  
12  
13  
14  
15  
16  
17  
18  
19  
20  
21  
22  
23  
24  
25  
26  
27  
28  
29  
30  
31  
32  
33  
34  
35  
36  
37  
38  
39  
40  
41  
42  
43  
44  
45  
46  
47  
48  
49  
50  
51  
52  
53  
54  
55  
56  
57  
58  
59  
60

# Tuning the Photoelectrocatalytic Hydrogen Evolution of Pt-decorated Silicon Photocathodes by Pt Electroless Deposition Temperature and Time

*Bruno Fabre<sup>a,\*</sup>, Li Gaozeng<sup>a</sup>, Francis Gouttefangeas<sup>b</sup>, Loic Joanny<sup>b</sup> and Gabriel Loget<sup>a,\*</sup>*

<sup>a</sup> Institut des Sciences Chimiques de Rennes (ISCR), UMR 6226 CNRS/Université de Rennes  
1, Matière Condensée et Systèmes Electroactifs (MaCSE), Campus de Beaulieu, 35042  
Rennes Cedex, France

<sup>b</sup> ScanMAT – CMEBA, Université de Rennes 1, Campus de Beaulieu, 35042 Rennes Cedex,  
France

KEYWORDS. Hydrogen evolution reaction; Hydrogen-terminated silicon; Electroless metal  
deposition; Photocathodes; Photoelectrocatalysis

ABSTRACT. The electroless deposition of Pt nanoparticles (NPs) on hydrogen-terminated  
silicon (H-Si) surfaces is studied as a function of temperature and the immersion time. It is  
demonstrated that isolated Pt structures can be produced at all investigated temperatures  
(between 22 and 75°C) for short deposition times, typically within 1-10 min if the  
temperature was 45°C or less than 5 min at 75°C. For longer times, dendritic metal structures

1  
2  
3 start to grow leading ultimately to highly rough interconnected Pt networks. Upon increasing  
4 temperature from 22 to 75°C and for an immersion time of 5 min, the average size of the  
5 observed Pt NPs monotonously increases from 120 to 250 nm and their number density  
6 calculated by scanning electron microscopy decreases from  $(4.5 \pm 1.0) \times 10^8$  to  $(2.0 \pm 0.5) \times$   
7  $10^8$  Pt NPs  $\text{cm}^{-2}$ . The impact of both the morphology and distribution of Pt nanoparticles on  
8 the photoelectrocatalytic activity of the resulting metallized photocathodes is then analyzed.  
9 Pt deposited at 45°C for 5 min yields photocathodes with the best electrocatalytic activity for  
10 the hydrogen evolution reaction (HER). Under illumination at 33  $\text{mW cm}^{-2}$ , this optimized  
11 photoelectrode shows a fill factor ( $FF$ ) of 45%, an efficiency ( $\eta$ ) of 9.7% and a short-circuit  
12 current density ( $|J_{sc}|$ ) at 0 V vs reversible hydrogen electrode (RHE) of 15.5  $\text{mA cm}^{-2}$ .  
13  
14  
15  
16  
17  
18  
19  
20  
21  
22  
23  
24  
25  
26  
27  
28  
29  
30

31 **1. Introduction.** The conversion of sunlight into clean and storable fuels is very appealing  
32 in the frame of the actual growing need for sustainable sources of energies. To this end, the  
33 use of solar-driven electrochemical cells that can split water into hydrogen and oxygen seems  
34 a very promising technology.<sup>1,2,3</sup> Nevertheless, the fabrication of stable, low-cost and really  
35 efficient photoelectrodes is still a harsh challenge in this thematic area.<sup>4,5,6,7</sup> Silicon, with a  
36 gap energy of 1.12 eV,<sup>8</sup> is a very promising material to be used as a photocathode material for  
37 hydrogen evolution reaction (HER) because of its abundance, non-toxicity and its tunable  
38 electronic properties.<sup>9</sup> However, slow charge transfer kinetics at bare Si and the high  
39 recombination rate of electron-hole pairs generated under illumination constitute serious  
40 obstacles to promote efficiently multielectron processes.<sup>9,10</sup> Therefore, the deposition of pure  
41 metals<sup>9</sup>, metal oxides or sulfides<sup>4,6,11,12</sup> onto silicon is an effective way to overcome the  
42 intrinsic problems of this semiconductor serving as a photocathode. Among the catalytically  
43 active metals, platinum is known as the most efficient electrocatalyst for HER which can  
44  
45  
46  
47  
48  
49  
50  
51  
52  
53  
54  
55  
56  
57  
58  
59  
60

1  
2  
3 remain stable either in acidic or alkaline electrolyte.<sup>9,13,14,15,16,17,18,19,20,21,22,23</sup> It has been  
4  
5 demonstrated that Pt, deposited in the form of nanoparticles (NPs), exhibited much higher  
6  
7 electrocatalytic activity than that of a continuous Pt film.<sup>9,24</sup> Furthermore, the catalytic  
8  
9 performances of Pt NPs were found to be highly dependent on their size, their morphology  
10  
11 and their shape.<sup>25,26,27,28,29,30</sup> In that context, attention has been paid to the development of  
12  
13 synthetic procedures directed towards the deposition of Pt NPs with high-index facets.<sup>31,32,33,34</sup>  
14  
15 Indeed, the high-index facets are usually more active in chemical reactions and heterogeneous  
16  
17 catalytic processes compared with the low-index planes of closely packed surface atoms. As a  
18  
19 matter of fact, a surface with high-index planes possesses a high density of terraced, stepped  
20  
21 and kinked sites which serve as active sites for a range of reactions. A common route for the  
22  
23 synthesis of such shape-controlled Pt NPs involves the gas-phase reduction of a precursor Pt  
24  
25 salt in the presence of a capping agent.<sup>26,27,35,36,37</sup> Electrochemical methods such as potential  
26  
27 cycling<sup>38</sup> and square-wave potential voltammetry<sup>31,39,40,41</sup> have also been successfully  
28  
29 employed for the deposition of Pt NPs with high-index facets onto glassy carbon and graphite  
30  
31 surfaces.  
32  
33  
34  
35  
36

37  
38 In the present work, we exploit another electrochemical approach, namely the electroless  
39  
40 deposition by galvanic displacement<sup>42,43</sup>, to grow Pt NPs with different shapes onto  
41  
42 photoactive silicon surfaces. In the past, this surfactant-free method has been demonstrated to  
43  
44 be a simple and fast procedure to yield Pt NPs-decorated semiconducting surfaces exhibiting  
45  
46 improved interfacial charge transfer rates and hydrogen evolution performances.<sup>14,17,18,19,22,23</sup>  
47  
48

49  
50 We demonstrate herein that both the morphology and the density of Pt nanoparticles deposited  
51  
52 on silicon can be finely tuned by electroless deposition temperature and time. In our study, a  
53  
54 wide range of temperature (20-75°C) and time (1-30 min) has been used to produce a large  
55  
56 palette of structurally different Pt nanostructures going from separated spherical nanoparticles  
57  
58 to interconnected dendritic structures. In contrast, most of reported electroless metal  
59  
60 deposition methods were conducted at ca. room temperature for a few minutes and a single

1  
2  
3 type of metal morphology was usually deposited. To the best of our knowledge, this is the  
4  
5 first time that the impact of both deposition temperature and time on the electrocatalytic  
6  
7 performance of the resulting metallized silicon photocathodes for HER has been addressed  
8  
9 with the goal of identifying the most efficient photocathode, in terms of short-circuit current  
10  
11 density ( $J_{sc}$ ), fill factor ( $FF$ ) and thermodynamic efficiency for production of  $H_2$  ( $\eta$ ).<sup>5</sup>  
12  
13  
14  
15  
16  
17

## 18 **2. Experimental**

19  
20 **2.1. Reagents.** Acetone (MOS electronic grade, Erbatron from Carlo Erba) and anhydrous  
21  
22 ethanol (RSE electronic grade, Erbatron from Carlo Erba) were used without further  
23  
24 purification. The chemicals used for the cleaning and etching of silicon wafer pieces (30%  
25  
26  $H_2O_2$ , 96-97%  $H_2SO_4$  and 50% HF solutions) were of VLSI ( $H_2O_2$ , from Sigma-Aldrich) and  
27  
28 MOS ( $H_2SO_4$  from O-BASF and HF from Sigma-Aldrich) semiconductor grade.  
29  
30  
31

32 **2.2. Preparation of Pt-decorated silicon surfaces.** A piece of *p*-type Si(100) (1-5  $\Omega$  cm  
33  
34 resistivity, boron doped, 250  $\mu$ m thickness, Siltronix) was sonicated for 10 minutes  
35  
36 successively in acetone, ethanol and ultra-pure 18.2 M $\Omega$  cm water (Veolia Water STI) to  
37  
38 degrease it. It was then cleaned with piranha solution (3:1 v/v concentrated  $H_2SO_4$ /30%  $H_2O_2$ )  
39  
40 for 30 min at 100°C, followed by copious rinsing with ultra-pure water to eliminate heavy  
41  
42 metals and organic residues.  
43  
44  
45

46 *Caution: The concentrated aqueous  $H_2SO_4/H_2O_2$  (piranha) solution is very dangerous,*  
47  
48 *particularly in contact with organic materials, and should be handled extremely carefully.*  
49

50 Hydrogen-terminated Si(100) (H-Si) was obtained by immersing the Si(100) substrate  
51  
52 previously decontaminated with piranha solution into HF 10% wt (~5.7 M) for 2 min,  
53  
54 followed by drying under an argon stream.  
55  
56

57 *Caution: Proper precautions must be used when handling hydrogen fluoride. Hydrogen*  
58  
59 *fluoride is extremely corrosive to human tissue, contact resulting in painful, slow-healing*  
60

1  
2  
3 *burns. Laboratory work with HF should be conducted only in an efficient hood, with the*  
4  
5  
6 *operator wearing a full-face shield and protective clothing.*

7  
8 Pt-coated silicon surfaces were obtained by electroless deposition in the presence of HF. A  
9  
10 freshly prepared H-Si sample was dipped for a time varying between 1 and 30 min into a  
11  
12 solution of Na<sub>2</sub>PtCl<sub>4</sub> (Strem Chemicals) at 1 mM in HF 10%. The metallic salt solution was  
13  
14 previously kept at rt or heated at 45°C, 60°C or 75°C for 30 min before the introduction of H-  
15  
16 Si and kept at the selected temperature throughout the course of the reaction. The metallized  
17  
18 surface was thoroughly rinsed with ultrapure water and dried under an argon stream. It was  
19  
20 then immediately used for (photo)electrochemical measurements.  
21  
22

23  
24 **2.3. Electrochemical Characterization.** All the electrochemical experiments were  
25  
26 performed in a home-made three-electrode glass cell comprising a quartz window. The  
27  
28 electrical contact with the working electrode was made by applying a drop of In-Ga eutectic  
29  
30 (Alfa Aesar, 99.99%) on the previously polished backside of the silicon electrode. KCl  
31  
32 saturated calomel electrode (SCE) was used as the reference electrode. A glassy carbon rod  
33  
34 was used as the counter electrode. Potentials vs SCE were converted into potentials vs  
35  
36 reversible hydrogen electrode (RHE) from measurements of the open-circuit potential (OCP)  
37  
38 of a clean Pt electrode in the pH 1 solution saturated with research grade H<sub>2</sub> (Air-Liquide,  
39  
40 99.999%). The OCP potential was measured to be  $-0.300 \pm 0.005$  V vs SCE, in close  
41  
42 agreement with the theoretically predicted value by the expression:  $V_{\text{RHE}} = V_{\text{SCE}} + 0.24 +$   
43  
44  $0.059 \cdot \text{pH}$ . All the linear sweep voltammograms were *iR*-corrected using the resistance  
45  
46 determined by impedance spectroscopy at high frequency (100 kHz). Typical values of  $26 \pm 5$   
47  
48 ohm were obtained for our different photoelectrochemical cells and were found to be not  
49  
50 really dependent on the type of metallized photoelectrode.  
51  
52

53  
54 *Electrochemical Measurements.* Linear sweep voltammetry (LSV) and chronoamperometry  
55  
56 were performed with an Autolab electrochemical analyzer (PGSTAT 30  
57  
58 potentiostat/galvanostat from Eco Chemie B.V.) equipped with the GPES and FRA software.  
59  
60

1  
2  
3 The aqueous solution containing sodium sulfate ( $\text{Na}_2\text{SO}_4$ , Carlo Erba, 99.6%) at 0.5 M was  
4  
5 adjusted to pH 1 with  $\text{H}_2\text{SO}_4$  and was continuously stirred with a stir bar during the  
6  
7 electrochemical measurements. We have checked that the addition of  $\text{Na}_2\text{SO}_4$  into the acidic  
8  
9 solution did affect neither the potential scale nor the photoelectrochemical measurements at  
10  
11 metallized H-Si photocathodes. The geometrical area of silicon exposed to light was  $0.2 \text{ cm}^2$ .  
12  
13 All the electrochemical measurements were carried out inside a home-made Faraday cage at  
14  
15 room temperature and under a constant flux of argon.  
16  
17

18  
19 **2.4. Additional Instrumentation.** *Light source.* The light source used for the  
20  
21 photoelectrochemical experiments with silicon electrodes was an optical fiber (Fiber Light  
22  
23 DC950H from Dolan Jenner), equipped with a 150 W quartz halogen. The fluence of the lamp  
24  
25 at the position occupied by the silicon working electrode was measured as  $33 \text{ mW cm}^{-2}$  by  
26  
27 using an optical power/energy meter (Model 842-PE, Newport) coupled to a silicon  
28  
29 photodiode (Model 918D-SL-OD3, Newport). This value corresponds to the maximum power  
30  
31 reached by our light source. A Xe lamp allowing illumination at  $100 \text{ mW cm}^{-2}$ , as traditionally  
32  
33 used in this kind of photoelectrocatalytic experiments, was not currently available in our lab.  
34  
35

36  
37 *Scanning Electron Microscopy.* A JEOL JSM-7100F Scanning Electron Microscope (SEM)  
38  
39 was used to analyze the morphology of Pt-coated silicon surfaces as a function of both the  
40  
41 metal deposition temperature and time. The images were processed by the ImageJ (version  
42  
43 1.45s) software to determine the number density of Pt particles deposited on H-Si(100)  
44  
45 surfaces. The procedure to count the Pt particles was as follows. First, the "Analyze/Set  
46  
47 Scale" dialog box was used to define the spatial scale from the scale bar in the SEM images.  
48  
49 The "Analyze particles" automated routine was then used to count and outline the Pt particles.  
50  
51 The data window was copied and pasted to a OriginPro 8.5 spreadsheet.  
52  
53  
54  
55  
56  
57

### 58 **3. Results and Discussion.**

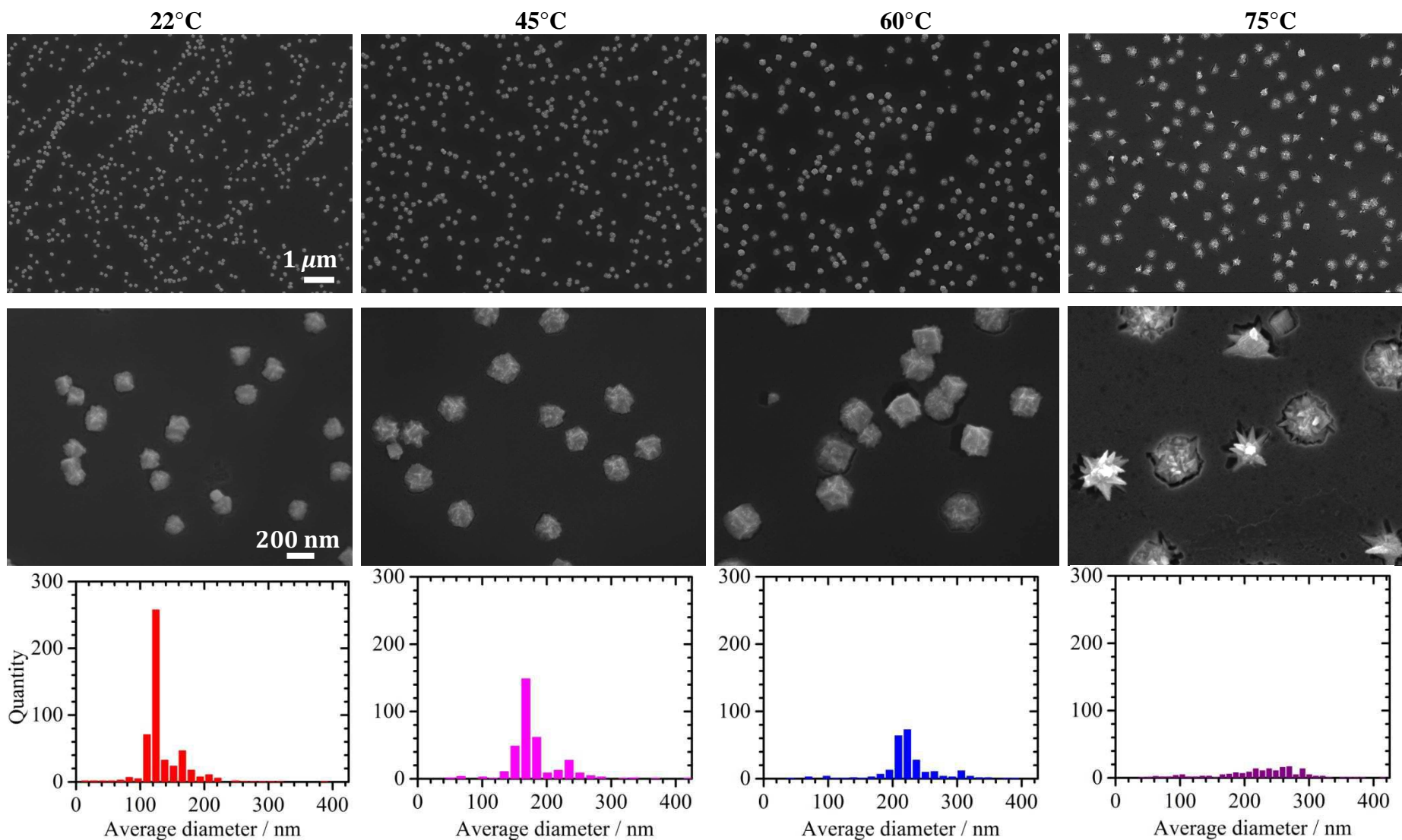
59  
60

1  
2  
3 *3.1. Morphology of the Pt NPs deposited on H-Si.* Figure 1 shows the SEM images of Pt  
4 NPs deposited on H-Si by electroless galvanic displacement at different temperatures for 5  
5 min from an aqueous HF-containing metallic solution at 1 mM. The Pt NPs were of  
6 hexoctahedron shape<sup>44</sup> when the deposition temperature was fixed between 22 and 60°C. For  
7 a temperature of 75°C, a mixture of hexaocahedra and highly branched structures was  
8 observed. Furthermore, the density of deposited Pt NPs decreased upon increasing the  
9 deposition temperature from 22 to 75°C. The number density calculated by SEM (Figure S1,  
10 Supporting Information) was around  $(4.5 \pm 1.0) \times 10^8$ ,  $(3.5 \pm 0.8) \times 10^8$ ,  $(3.0 \pm 0.6) \times 10^8$  and  
11  $(2.0 \pm 0.5) \times 10^8$  Pt NPs per cm<sup>2</sup> of the silicon surface at 22, 45, 60 and 75°C, respectively.  
12 Moreover, the average size of the observed features monotonously increased from 120 to 250  
13 nm within this temperature range with an approximately constant size distribution until 60°C  
14 enlarging at 75°C (the width at half-maximum was found to be  $35 \pm 5$  nm within the 22-60°C  
15 range and increased to  $120 \pm 10$  nm at 75°C). It is worth mentioning that the average surface  
16 occupied by the Pt particles was determined to be around  $9 \pm 1\%$  of the total silicon surface  
17 and was found to be not significantly dependent on the deposition temperature. For all  
18 investigated temperatures, the metal deposition mechanism involved the attack of the bulk  
19 silicon concomitantly with the growth of isolated Pt NPs which resulted ultimately in the  
20 formation of nanotrenches surrounding the Pt NPs (Figures 1 and S2). The morphology of the  
21 grown Pt NPs was not only dependent on the deposition temperature but also on the  
22 immersion time. The latter parameter has been examined more in detail for two representative  
23 temperatures: 45 and 75°C. For 45°C, Pt NPs were essentially of hexoctahedron shape when  
24 the deposition time did not exceed 10 min. For times longer than 15 min, highly branched  
25 structures, grown from the corners of the polyhedral, were observed leading to the formation  
26 of a few hundred nm long Pt dendrites after 30 min deposition (Figure 2). When the  
27 temperature was fixed at 75°C, the transition between hexoctahedron and highly branched  
28  
29  
30  
31  
32  
33  
34  
35  
36  
37  
38  
39  
40  
41  
42  
43  
44  
45  
46  
47  
48  
49  
50  
51  
52  
53  
54  
55  
56  
57  
58  
59  
60

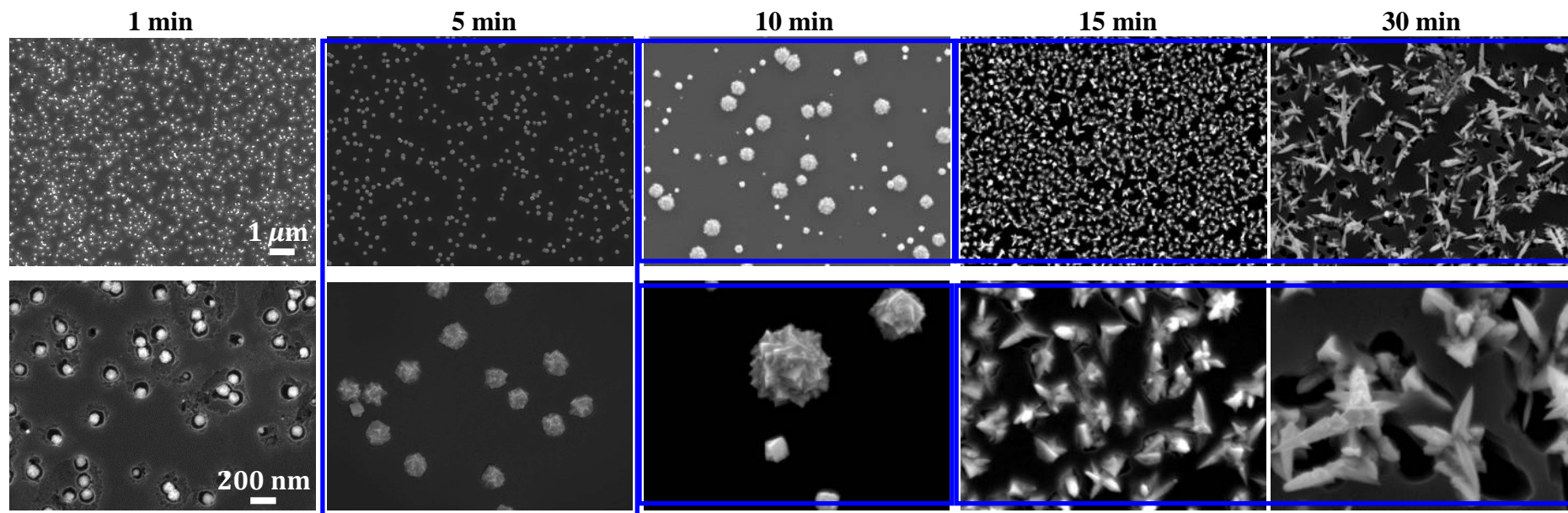
1  
2  
3 structures occurred at shorter times, between 1 and 5 min. Long dendrites standing out of  
4  
5 silicon trenches were clearly visible from 10 min (Figure 3).  
6  
7

8 To sum-up, isolated Pt structures can be produced at all investigated temperatures for short  
9  
10 deposition times, typically within 1-10 min if the temperature was 45°C or less than 5 min at  
11  
12 75°C. For longer times, dendritic metal structures start to grow leading ultimately to highly  
13  
14 rough interconnected Pt networks. As detailed in the next section, such differences in both the  
15  
16 morphology and the density of deposited Pt NPs have a strong impact on the electrocatalytic  
17  
18 performances for HER of metallized surfaces.  
19  
20  
21  
22  
23  
24  
25  
26  
27  
28  
29  
30  
31  
32  
33  
34  
35  
36  
37  
38  
39  
40  
41  
42  
43  
44  
45  
46  
47  
48  
49  
50  
51  
52  
53  
54  
55  
56  
57  
58  
59  
60

1  
2  
3  
4  
5  
6  
7  
8  
9  
10  
11  
12  
13  
14  
15  
16  
17  
18  
19  
20  
21  
22  
23  
24  
25  
26  
27  
28  
29  
30  
31  
32  
33  
34  
35  
36  
37  
38  
39  
40  
41  
42  
43  
44  
45  
46  
47



1  
2  
3 **Figure 1.** (Top, middle) SEM Images of flat H-Si(100) surfaces after electroless deposition of Pt at different temperatures for 5 min. Deposition  
4 solution:  $\text{Na}_2\text{PtCl}_4$  at 1 mM in HF 5.7 M. (Bottom) Corresponding particle size distributions.  
5  
6  
7  
8  
9



31 **Figure 2.** SEM Images of flat H-Si(100) surfaces after electroless deposition of Pt at 45°C for 1, 5, 10, 15 and 30 min. Deposition solution:  
32  $\text{Na}_2\text{PtCl}_4$  at 1 mM in HF 5.7 M.  
33  
34  
35  
36  
37  
38  
39  
40  
41  
42  
43  
44  
45  
46  
47

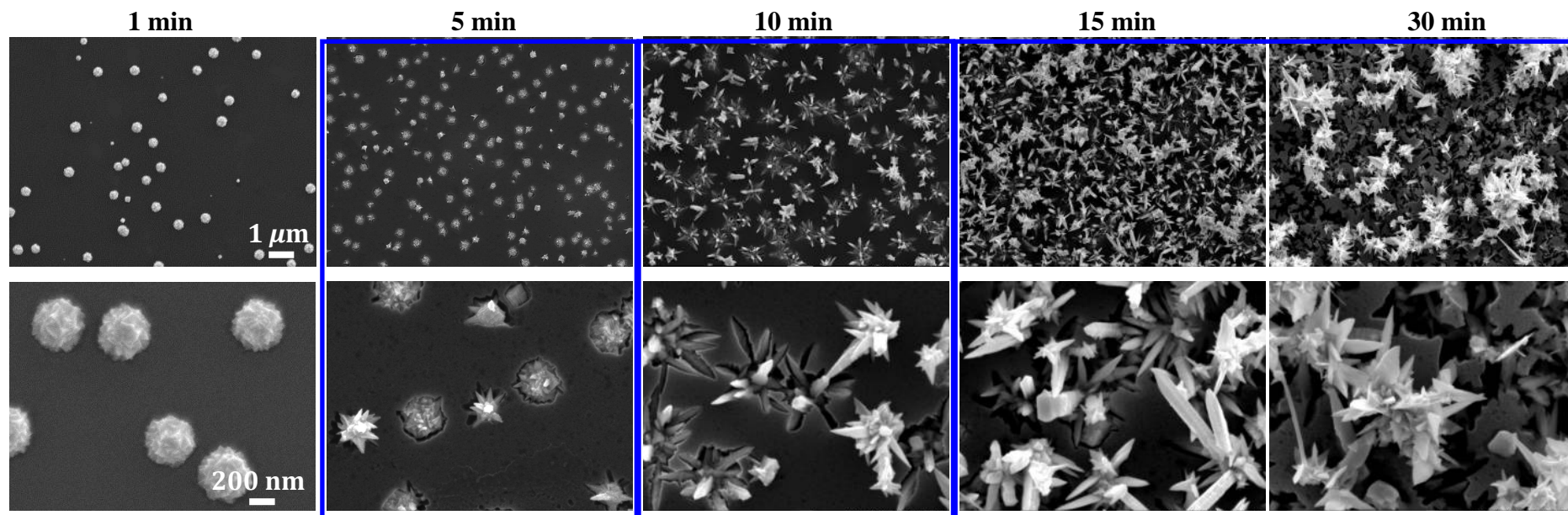


**Figure 3.** SEM Images of flat H-Si(100) surfaces after electroless deposition of Pt at 75°C for 1, 5, 10, 15 and 30 min. Deposition solution:

Na<sub>2</sub>PtCl<sub>4</sub> at 1 mM in HF 5.7 M.

1  
2  
3  
4  
5  
6  
7  
8  
9  
10  
11  
12  
13  
14  
15  
16  
17  
18  
19  
20  
21  
22  
23  
24  
25  
26  
27  
28  
29  
30  
31  
32  
33  
34  
35  
36  
37  
38  
39  
40  
41  
42  
43  
44  
45  
46  
47  
48  
49  
50  
51  
52  
53  
54  
55  
56  
57  
58  
59  
60

3.2. *Electrocatalytic HER at platinized H-Si photocathodes.* Figure 4 shows the  $iR$ -corrected polarization curves obtained at Si photocathodes which had been previously metallized at different temperatures for 5 min. As expected, no appreciable reduction current was measured in the dark for all the electrodes. Under illumination with a halogen lamp ( $33 \text{ mW cm}^{-2}$ ), they exhibited much higher electrocatalytic performance than that of nonmetallized H-Si(100). For example, the overpotential for hydrogen evolution was significantly decreased by ca. 940 mV with respect to H-Si(100) (measured for a current density of  $5.0 \text{ mA cm}^{-2}$ ) under identical illumination conditions. We now examine in more details the effects of the metal deposition temperature on the electrocatalytic behavior of the photoelectrodes. Qualitatively, the cathodic photocurrent densities corresponding to HER were significantly higher at photocathodes metallized at temperatures above  $45^\circ\text{C}$ . In contrast, the open-circuit voltage  $V_{oc}$  (the difference between the potential at which the photoelectrode passed no current and the formal potential of the  $\text{H}^+/\text{H}_2$  redox couple)<sup>5</sup> was constant at  $450 \pm 10 \text{ mV vs RHE}$  and not dependent on the deposition temperature. For all the metallized photoelectrodes, it is worth noting that the catalytic photocurrent decreased slightly for potentials below  $0.0 \text{ V vs RHE}$  instead of being flat as expected for light-limited catalytic current. Such a trend is thought to be due to the gradual decrease in the active surface area of the photoelectrode caused by the accumulation of  $\text{H}_2$  bubbles which were not totally removed from the surface upon stirring.

To evaluate quantitatively the respective catalytic performance of each metallized electrode, two other characteristic parameters have been determined, namely the fill factor ( $FF$ , eq 1) and the thermodynamic efficiency for  $\text{H}_2$  evolution ( $\eta$ , eq 2).<sup>5</sup>

$$FF = \frac{P_{\max}}{V_{oc} \cdot |J_{sc}|} \quad (1)$$

$$\eta = \frac{P_{\max}}{P_{\text{in}}} = \frac{FF \cdot V_{\text{oc}} \cdot |J_{\text{sc}}|}{P_{\text{in}}} \quad (2)$$

where  $P_{\max}$  is the maximum product of  $|j|$  and  $E$ ,  $|J_{\text{sc}}|$  is the short-circuit current density (at  $E = 0 \text{ V vs RHE}$ ) and  $P_{\text{in}}$  is the incoming light intensity (i.e.  $33 \text{ mW cm}^{-2}$ ). The results are gathered in Figure 5. The values of  $FF$  (25%),  $\eta$  ( $<0.01\%$ ) and  $|J_{\text{sc}}|$  ( $0.02 \text{ mA cm}^{-2}$  at  $0 \text{ V vs RHE}$ ) calculated for H-Si are consistent with the poor activity of this photoelectrode for HER. In contrast, the photoelectrodes metallized at temperatures between  $45$  and  $75^\circ\text{C}$  were the most active with comparable  $FF$  (40-45%),  $\eta$  (9-10%) and  $|J_{\text{sc}}|$  ( $14.5$ - $15.5 \text{ mA cm}^{-2}$ ). The surface metallized at  $22^\circ\text{C}$  exhibited a lower HER activity, as supported by smaller  $\eta$  (6.7%) and  $|J_{\text{sc}}|$  ( $12 \text{ mA cm}^{-2}$ ).

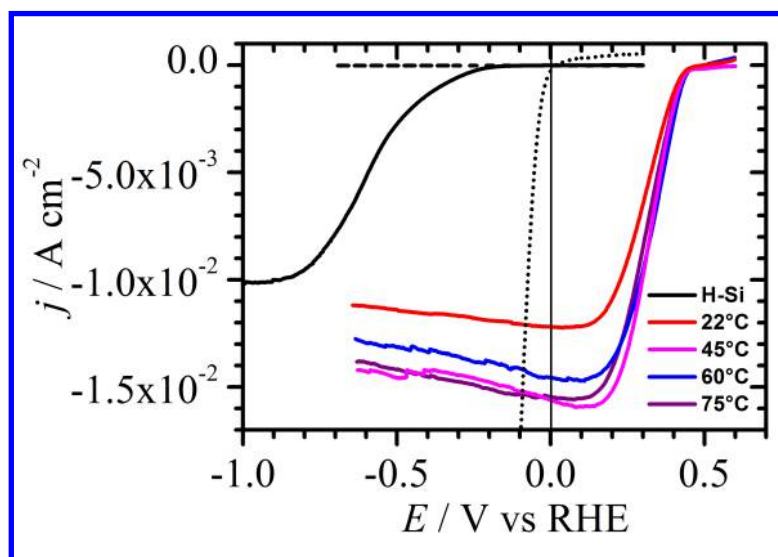


**Figure 4.** Linear sweep voltammograms at  $20 \text{ mV s}^{-1}$  of Pt-coated Si(100) electrodes in  $\text{H}_2\text{SO}_4$  solution containing  $0.5 \text{ M Na}_2\text{SO}_4$  (pH 1), in the dark (dashed trace) and under illumination (solid traces). Pt was electroless deposited at different temperatures for 5 min from a HF  $5.7 \text{ M}$  solution containing  $\text{Na}_2\text{PtCl}_4$  at  $1 \text{ mM}$ . The black solid and dotted traces correspond to the response of bare H-Si under illumination and Pt disk electrode, respectively.

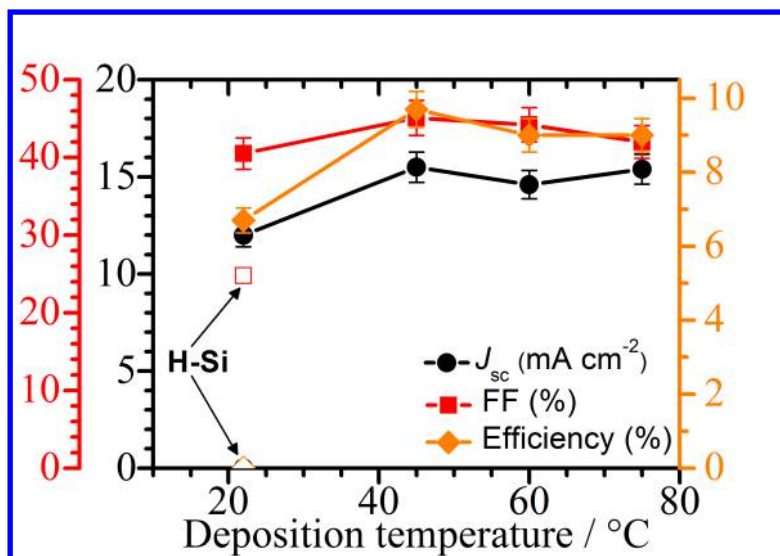


**Figure 5.** Figures of merit of photocathodes metallized at different temperatures for 5 min.

The polarization curves of the silicon photoelectrodes metallized at two representative temperatures, namely 45 and 75°C, for different times are shown in Figures 6 and 7. For 45°C,  $V_{oc}$  was found to increase from 320 to 450 mV vs RHE upon increasing deposition time from 1 to 5 min, then remained approximately constant at  $(450 \pm 20)$  mV for longer times. The  $FF$ ,  $\eta$  and  $|J_{sc}|$  values calculated as a function of the deposition time (Figure 8) demonstrated that the photoelectrode metallized for 5 min exhibited the best catalytic activity ( $FF = 45\%$ ,  $\eta = 9.7\%$  and  $|J_{sc}| = 15.5 \text{ mA cm}^{-2}$ ). Times smaller than 3 min were found to yield less active photoelectrodes with smaller  $FF$  (18-30%),  $\eta$  (2.2-5.0%) and  $|J_{sc}|$  (12.5-14.4  $\text{mA cm}^{-2}$ ) values. The photoelectrodes metallized for times longer than 15 min exhibited catalytic performances which were only slightly lower than those obtained for the photoelectrode metallized for 5 min. Such a situation can be partially explained by the concomitant formation of nanotrenches in the silicon bulk and the growth of branched Pt structures (Figure 2). As previously suggested, enlarging the semiconductor/metal junction area deep toward the bulk would lead to improved efficiencies.<sup>9</sup>

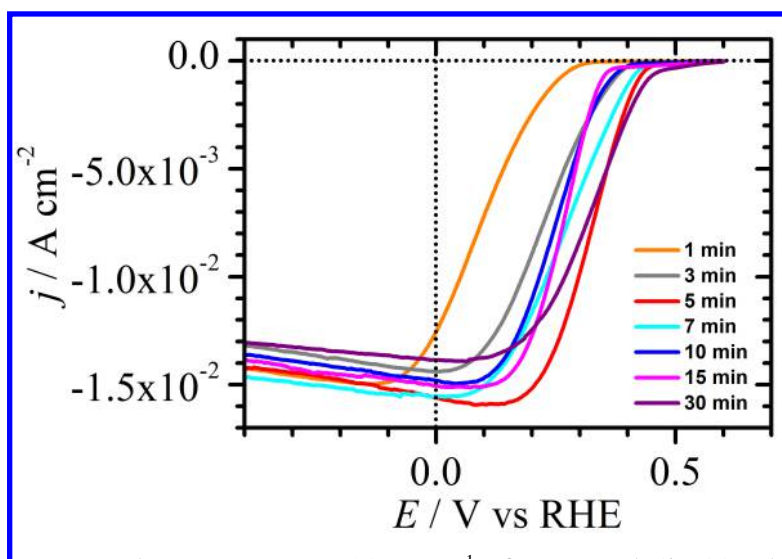


**Figure 6.** Linear sweep voltammograms at  $20 \text{ mV s}^{-1}$  of Pt-coated Si(100) electrodes in  $\text{H}_2\text{SO}_4$  solution containing  $0.5 \text{ M Na}_2\text{SO}_4$  (pH 1) under illumination. Pt was electroless deposited at  $45^\circ\text{C}$  for different times from a  $\text{HF } 5.7 \text{ M}$  solution containing  $\text{Na}_2\text{PtCl}_4$  at  $1 \text{ mM}$ .

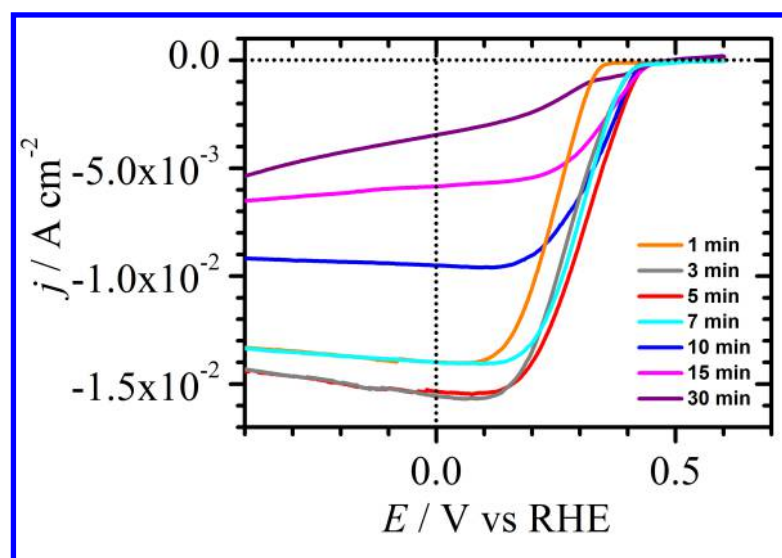


**Figure 7.** Linear sweep voltammograms at  $20 \text{ mV s}^{-1}$  of Pt-coated Si(100) electrodes in  $\text{H}_2\text{SO}_4$  solution containing  $0.5 \text{ M Na}_2\text{SO}_4$  (pH 1) under illumination. Pt was electroless deposited at  $75^\circ\text{C}$  for different times from a  $\text{HF } 5.7 \text{ M}$  solution containing  $\text{Na}_2\text{PtCl}_4$  at  $1 \text{ mM}$ .

1  
2  
3  
4  
5  
6  
7  
8  
9  
10  
11  
12  
13  
14  
15  
16  
17  
18  
19  
20  
21  
22  
23  
24  
25  
26  
27  
28  
29  
30  
31  
32  
33  
34  
35  
36  
37  
38  
39  
40  
41  
42  
43  
44  
45  
46  
47  
48  
49  
50  
51  
52  
53  
54  
55  
56  
57  
58  
59  
60

As seen in the SEM pictures, the formation of nanotrenches was observed at shorter deposition times (less than 5 min) when the surface was metallized at 75°C. As a result, the catalytic performances of the surfaces metallized at this temperature for 1 and 3 min were higher than those metallized at 45°C for the same times (Figure 8).  $V_{oc}$  was raised from 355 to 450 mV by increasing the time from 1 to 3 min, then remained constant at approximately  $(450 \pm 20)$  mV for longer times. The best compromise between catalytic efficiency and photocurrent was obtained for an optimal deposition time of 5 min ( $FF = 42\%$ ,  $\eta = 9.0\%$  and  $|J_{sc}| = 15.4 \text{ mA cm}^{-2}$ ). The catalytic activity of such a photoelectrode was quite similar to that of the best photoelectrode produced at 45°C for 5 min. However, in contrast with the surfaces metallized at 45°C,  $J_{sc}$  and  $\eta$  were found to decrease dramatically for times exceeding 10 min. Three possible reasons can be involved to explain such a trend. First, it is very likely that the density of surface defects increases with the deposition time and these sites act as recombination centers of the photogenerated charge carriers lowering the overall catalytic efficiency.<sup>9</sup> The second one is related to the high coverage of the Pt layer from 15 min (as supported by SEM, Figure 3) which would limit the amount of light absorbed by silicon and thus would reduce the photocurrent.<sup>5,15</sup> The third one concerns the less efficient injection of photogenerated charge carriers with the progressive conversion of the metal layer from well-dispersed and isolated islands at short times to an interconnected metal structure for times longer than 15 min.

The UV-visible reflectance measurements performed with surfaces metallized at 45 and 75°C indicate that the light-harvesting properties of these surfaces were globally improved upon increasing the deposition time (Figure S3, Supporting Information). Consequently, the decrease of the catalytic properties of the photoelectrodes obtained at long deposition times would

probably result from accelerated charge recombination and less efficient charge injection phenomena.

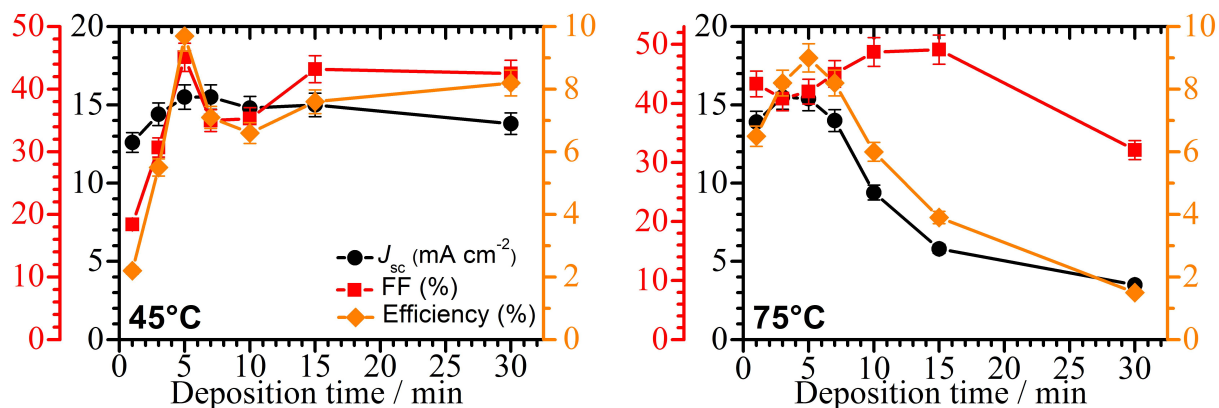


**Figure 8.** Catalytic performances of the Pt-coated photoelectrodes as a function of the Pt deposition temperature (deposition time: 5 min). The continuous lines are a guide for the eyes.

**3.3. Stability of the optimized photoelectrode for HER.** The photoelectrode exhibiting the best electrocatalytic efficiency (namely, that prepared at 45°C for 5 min) was tested over one hour at 0.0 V vs RHE under illumination (33 mW cm<sup>-2</sup>). As shown in Figure 9, the photocurrent produced with this photoelectrode remained relatively stable during the electrolysis time. The amount of H<sub>2</sub> produced was determined from the gas volume by measuring the amount of the electrolytic solution displaced in a sealed and graduated upside-down burette (Hoffman cell).<sup>45</sup> H<sub>2</sub> was evolved with a constant rate of 110 ± 20 μmol h<sup>-1</sup> and a Faradaic yield >90%. O<sub>2</sub> evolution at the Pt counter electrode was also monitored and the overall molar ratio of the evolved H<sub>2</sub>:O<sub>2</sub> was 2.5 ± 0.2 (Figure 9b). These deviations from the expected Faradaic yield of 100 % and stoichiometric ratio of 2:1 are believed to be due to the uncertainty in the gas volume measurements with the Hoffman cell and to a possible reduction of a small fraction of the O<sub>2</sub>

generated at the anode. However, these results clearly show that such photocathode is robust enough to be operated for H<sub>2</sub> production during a reasonable amount of time.

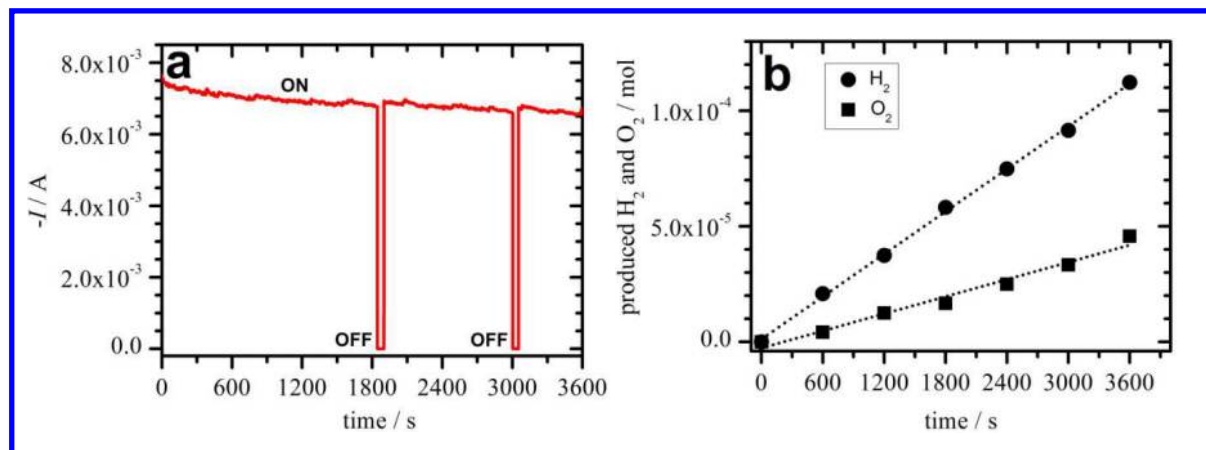


**Figure 9.** (a) Current-time curve obtained by controlled-potential electrolysis at 0.0 V vs RHE for the photoelectrode prepared at 45°C for 5 min in H<sub>2</sub>SO<sub>4</sub> solution containing 0.5 M Na<sub>2</sub>SO<sub>4</sub> (pH 1) under illumination at 33 mW cm<sup>-2</sup> (ON state) with two dark periods (OFF state). (b) Amount of H<sub>2</sub> and O<sub>2</sub> evolved at the photoelectrode and the Pt counter electrode, respectively, as a function of the electrolysis time. The number of mole of produced gas was calculated from gas volume in a Hoffman cell.

*3.4. Comparison with other Pt NPs-decorated H-Si photocathodes.* Table 1 lists the reported HER performances of several Pt-metallized Si photocathodes using different deposition methods (electroless, electrochemical, evaporation and atomic layer deposition ALD). Two types of electrode structures have been considered, namely planar and micro-/nanostructured silicon. Globally, the optimized photoelectrode prepared in this study exhibits the best catalytic activity, in terms of  $V_{oc}$ ,  $FF$  and  $\eta$ , compared with other photoelectrodes based on planar silicon. The smaller value of  $J_{sc}$  found herein can be reasonably ascribed to the lower illumination power.

1  
2  
3  
4  
5  
6 From Table 1, it is also evident that the electrochemical deposition methods failed to produce  
7  
8 photocathodes with high  $V_{oc}$  and  $\eta$ . Moreover, it is worth mentioning that the exceptional  
9  
10 efficiency reported by Lombardi et al. ( $>10\%$ )<sup>15</sup> has been calculated for a three-electrode  
11  
12 electrochemical cell using the expression available for a complete water splitting photoelectrode  
13  
14 device<sup>5</sup> and consequently is an overestimate of the real efficiency of the individual HER  
15  
16 photocathode. Compared with structured photoelectrodes, our optimized planar photocathode  
17  
18 exhibits a comparable or higher catalytic performance. The use of Si micro- and nanowires as  
19  
20 electrode materials was found to significantly improve  $V_{oc}$  relative to the planar electrodes.  
21  
22 Nevertheless, the measured photocurrent densities were not significantly enhanced as expected  
23  
24 for such high surface area structures. This well-known trend has been attributed to a less efficient  
25  
26 light absorption by the wires essentially due to the high density of surface states.<sup>9</sup> Furthermore,  
27  
28 the use of a high-cost metal deposition technique, such as atomic layer deposition (ALD),  
29  
30 yielded photocathodes with small  $J_{sc}$  and  $\eta$ , in spite of a uniform distribution of Pt NPs along the  
31  
32 wires.<sup>20</sup> As a matter of fact, the only configuration allowing outstanding HER performance  
33  
34 included a  $n^+p$  radial junction in planar or Si wire-array structures.<sup>18</sup>  $FF$  higher than 50% with  
35  
36  $V_{oc}$  of ca. 0.55 V vs RHE were measured for such photoelectrodes.  
37  
38  
39  
40  
41  
42  
43  
44  
45  
46  
47  
48  
49  
50  
51  
52  
53  
54  
55  
56  
57  
58  
59  
60

**Table 1.** Key HER catalytic parameters for different Pt metallized silicon photocathodes.

Pt deposition method <sup>a</sup>	Pt deposition conditions	Illumination power / mW cm <sup>-2</sup>	pH	V <sub>oc</sub> / V vs RHE	-J <sub>sc</sub> / mA cm <sup>-2</sup>	FF / %	η / %	Ref.
<b>Planar p-Si</b>								
EL	5 min@45°C	33	1	0.46	15.5	45	9.7	This work
EL	3-8 min@rt	100	4.5	0.21-0.25	10-22	12-22	0.3-1.1	17
Echem	-2 V <sup>b</sup> for 4.5 s	100	4.5	0.27	21.5	33	1.9	16
EL	2-10 min@rt	10-100	1	-0.30	2-20 <sup>c</sup>	— <sup>d</sup>	25-10 <sup>c,e</sup>	15
EL	~10 min@rt	100	2	0.30	23	30	2.1	18
Echem	-0.3 V <sup>f</sup>	6.4-11.8 <sup>g</sup>	1.3	0.26	0.8 <sup>h</sup>	— <sup>d</sup>	2.7-3.5	13
<b>Micro-/Nanostructured p-Si</b>								
EL	~10 min@rt	100	2	0.16	7.3	18	21	18
EL	1 min@rt	100	0	-0.40	28	— <sup>d</sup>	— <sup>d</sup>	19
EL	3 × 3 min@rt	100	1	0.28	23	28	1.8	20
ALD	50 cycles @250°C	100	1	0.31	9	55	1.5	20
EL	3 min@rt	100	1	0.42	18	— <sup>d</sup>	— <sup>d</sup>	22
EL	10-20 min@rt	100	1	-0.40	20-25	— <sup>d</sup>	— <sup>d</sup>	23
<b>Planar n<sup>+</sup> p-Si</b>								
EBE	~ 6 × 10 <sup>-6</sup> torr pressure	100	2	0.56	28	60	~10.0	18
<b>Microwires n<sup>+</sup> p-Si</b>								
EBE	~ 6 × 10 <sup>-6</sup> torr pressure	100	2	0.54	15	71	~6.0	18

<sup>a</sup> EBE: electron-beam evaporation; EL: electroless; Echem: electrochemistry; ALD: atomic layer deposition. <sup>b</sup> Vs Ag/AgCl. <sup>c</sup> Measured at different illumination powers from 10 to 100 mW cm<sup>-2</sup>. <sup>d</sup> Not indicated. <sup>e</sup> Conversion efficiency for a complete water splitting photoelectrode device. <sup>f</sup> Vs SCE; Pt was deposited by passing ~30 mC cm<sup>-2</sup>

1  
2  
3  
4  
5  
6 of cathodic charge. <sup>g</sup> 632.8-nm light. <sup>h</sup> Calculated from photocurrent values and the 3-mm diameter of the  
7 photoelectrode.  
8  
9

10  
11  
12  
13 **4. Conclusions.** In this work, Pt-metallized silicon photoelectrodes, highly active for HER  
14 were fabricated by using the cost effective electroless deposition method by galvanic  
15 displacement. It was demonstrated that the morphology, the particle size and the surface  
16 distribution could be finely tuned by controlling the metal deposition temperature and time.  
17 Isolated Pt structures were produced at all investigated temperatures for short deposition times,  
18 typically within 1-10 min if the temperature was 45°C or less than 5 min at 75°C. The formation  
19 of multifaceted isolated Pt islands and nanotrenches into the silicon bulk were found to be  
20 beneficial for improving the catalytic performance of the photoelectrodes for HER. In contrast,  
21 the HER performance strongly decreased for photoelectrodes incorporating a high Pt loading  
22 with interconnected dendritic structures. The best catalytic performance was obtained for a  
23 photoelectrode which had been previously metallized at 45°C for 5 min. Such a photoelectrode  
24 was highly active for HER at pH 1 with outstanding output characteristics ( $FF = 45\%$ ,  $\eta = 9.7\%$   
25 and  $|J_{sc}| = 15.5 \text{ mA cm}^{-2}$ ) under a light illumination of  $33 \text{ mW cm}^{-2}$ . Such performances could be  
26 even improved by using Si structured surfaces incorporating an additional  $n^+$  Si layer on the p-  
27 type Si surface of the photocathode structure. Work directed towards this stimulating prospect is  
28 currently underway in our laboratory.  
29  
30  
31  
32  
33  
34  
35  
36  
37  
38  
39  
40  
41  
42  
43  
44  
45  
46  
47  
48  
49  
50

51  
52  
53 **Supporting Information.** Additional SEM images and total reflectance spectra of Pt-coated  
54 photoelectrodes. This material is available free of charge via the Internet at <http://pubs.acs.org>.  
55  
56  
57  
58  
59  
60

1  
2  
3  
4  
5  
6  
7  
8  
9  
10  
11  
12  
13  
14  
15  
16  
17  
18  
19  
20  
21  
22  
23  
24  
25  
26  
27  
28  
29  
30  
31  
32  
33  
34  
35  
36  
37  
38  
39  
40  
41  
42  
43  
44  
45  
46  
47  
48  
49  
50  
51  
52  
53  
54  
55  
56  
57  
58  
59  
60

## AUTHOR INFORMATION

### Corresponding Author

\*E-mail: bruno.fabre@univ-rennes1.fr (B.F.). Tel: +33 (0) 223 236 550. Fax: +33 (0) 223 236 797.

\* E-mail: gabriel.loget@univ-rennes1.fr (G. L.)

### Author Contributions

B. Fabre and G. Loget designed research, analyzed the electrochemical data and wrote the paper.

L. Gaozeng performed research. F. Gouttefangeas and L. Joanny performed the SEM characterizations and analyzed the SEM data. All authors have given approval to the final version of the manuscript.

### Notes

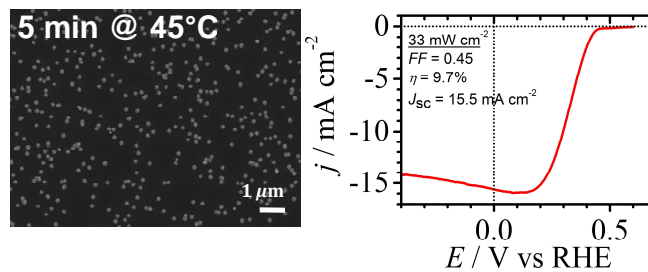
The authors declare no competing financial interest.

## ACKNOWLEDGMENT

The authors acknowledge CNRS and the Université de Rennes for support. F. Gouttefangeas and L. Joanny are also grateful to the Région Bretagne and European Union (CPER-FEDER 2007-2014) for financial support for SEM characterizations.

1  
2  
3  
4  
5  
6  
7  
8  
9  
10  
11  
12  
13  
14  
15  
16  
17  
18  
19  
20  
21  
22  
23  
24  
25  
26  
27  
28  
29  
30  
31  
32  
33  
34  
35  
36  
37  
38  
39  
40  
41  
42  
43  
44  
45  
46  
47  
48  
49  
50  
51  
52  
53  
54  
55  
56  
57  
58  
59  
60

## Table of Contents Graphic



## REFERENCES

- 
- (1) Cook, T. R.; Dogutan, D. K.; Reece, S. Y.; Surendranath, Y.; Teets, T. S.; Nocera, D. C. Solar Energy Supply and Storage for the Legacy and Nonlegacy Worlds. *Chem. Rev.* **2010**, *110*, 6474-6502.
- (2) Lewis, N. S.; Nocera, D. G. Powering the Planet: Chemical Challenges in Solar Energy Utilization. *Proc. Natl. Acad. Sci. USA* **2006**, *103*, 15729-15735.
- (3) Sivula, K.; van de Krol, R. Semiconducting Materials for Photoelectrochemical Energy Conversion. *Nat. Rev. Mater.* **2016**, *1*, 1-16.
- (4) Kang, D.; Kim, T. W.; Kubota, S. R.; Cardiel, A. C.; Cha, H. G.; Choi, K.-S. Electrochemical Synthesis of Photoelectrodes and Catalysts for Use in Solar Water Splitting. *Chem. Rev.* **2015**, *115*, 12839-12887.
- (5) Walter, M. G.; Warren, E. L.; McKone, J. R.; Boettcher, S. W.; Mi, Q.; Santori, E. A.; Lewis, N. S. Solar Water Splitting Cells. *Chem. Rev.* **2010**, *110*, 6446-6473.
- (6) Huang, Q.; Ye, Z.; Xiao, X. Recent Progress in Photocathodes for Hydrogen Evolution. *J. Mater. Chem. A* **2015**, *3*, 15824-15837.
- (7) Weber, M. F.; Dignam, M. J. Splitting Water with Semiconducting Photoelectrodes—Efficiency Considerations. *Int. J. Hydrogen Energy* **1986**, *11*, 225-232.
- (8) Zhang, X. G. In *Electrochemistry of Silicon and its Oxide*. Kluwer Academic Publishers: New York, 2004.
- (9) Sun, K.; Shen, S.; Liang, Y.; Burrows, P. E.; Mao, S. S.; Wang, D. Enabling Silicon for Solar-Fuel Production. *Chem. Rev.* **2014**, *114*, 8662-8719.

- 
- 1  
2  
3  
4  
5  
6  
7  
8 (10) Wrighton, M. S. Thermodynamics and Kinetics Associated with Semiconductor Based  
9 Photoelectrochemical Cells for the Conversion of Light to Chemical Energy. *Pure Appl. Chem.*  
10 **1985**, *57*, 57-68.  
11  
12  
13  
14 (11) Morales-Guio, C. G.; Hu, X. Amorphous Molybdenum Sulfides as Hydrogen Evolution  
15 Catalysts. *Acc. Chem. Res.* **2014**, *47*, 2671-2681.  
16  
17  
18 (12) Hou, Y.; Abrams, B. L.; Vesborg, P. C. K.; Björketun, M. E.; Herbst, K.; Bech, L.; Setti, A.  
19 M.; Damsgaard, C. D.; Pedersen, T.; Hansen, O.; Rossmeisl, J.; Dahl, S.; Norskov, J. K.;  
20 Chorkendorff, I. Bioinspired Molecular Co-Catalysts Bonded to a Silicon Photocathode for Solar  
21 Hydrogen Evolution. *Nature Mater.* **2011**, *10*, 434-438.  
22  
23  
24 (13) Dominey, R. N.; Lewis, N. S.; Bruce, J. A.; Bookbinder, D. C.; Wrighton, M. S.  
25 Improvement of Photoelectrochemical Hydrogen Generation by Surface Modification of p-Type  
26 Silicon Semiconductor Photocathodes. *J. Am. Chem. Soc.* **1982**, *104*, 467-482.  
27  
28  
29 (14) Szklarczyk, M.; Bockris, J. O. M. Photoelectrocatalysis and Electrocatalysis on p-Silicon. *J.*  
30 *Phys. Chem.* **1984**, *88*, 1808-1815.  
31  
32  
33 (15) Lombardi, I.; Marchionna, S.; Zangari, G.; Pizzini, S. Effect of Pt Particle Size and  
34 Distribution on Photoelectrochemical Hydrogen Evolution by p-Si Photocathodes. *Langmuir*  
35 **2007**, *23*, 12413-12420.  
36  
37  
38 (16) Huang, Z.; McKone, J. R.; Xiang, C.; Grimm, R. L.; Warren, E. L.; Spurgeon, J. M.;  
39 Lewerenz, H.-J.; Brunschwig, B. S.; Lewis, N. S. Comparison between the Measured and  
40 Modeled Hydrogen-Evolution Activity of Ni- or Pt-coated Silicon Photocathodes. *Int. J.*  
41 *Hydrogen Energy* **2014**, *39*, 16220-16226.  
42  
43  
44  
45  
46  
47  
48  
49  
50  
51  
52  
53  
54  
55  
56  
57  
58  
59  
60

- 
- 1  
2  
3  
4  
5  
6  
7  
8 (17) McKone, J. R.; Warren, E. L.; Bierman, M. J.; Boettcher, S. W.; Brunschwig, B. S.; Lewis,  
9 N. S.; Gray, H. B. Evaluation of Pt, Ni and Ni-Mo Electrocatalysts for Hydrogen Evolution on  
10 Crystalline Si Electrodes. *Energy Environ. Sci.* **2011**, *4*, 3573-3583.  
11  
12  
13  
14  
15 (18) Boettcher, S. W.; Warren, E. L.; Putnam, M. C.; Santori, E. A.; Turner-Evans, D.;  
16 Kelzenberg, M. D.; Walter, M. G.; McKone, J. R.; Brunschwig, B. S.; Atwater, H. A.; Lewis, N.  
17 S. Photoelectrochemical Hydrogen Evolution Using Si Microwire Arrays. *J. Am. Chem. Soc.*  
18 **2011**, *133*, 1216-1219.  
19  
20  
21  
22  
23  
24 (19) Zhao, Y.; Anderson, N. C.; Zhu, K.; Aguiar, J. A.; Seabold, J. A.; van de Lagemaat, J.;  
25 Branz, H. M.; Neale, N. R. Oxidatively Stable Nanoporous Silicon Photocathodes with Enhanced  
26 Onset Voltage for Photoelectrochemical Proton Reduction. *Nano Lett.* **2015**, *15*, 2517-2525.  
27  
28  
29  
30  
31 (20) Dai, P.; Xie, J.; Mayer, M. T.; Yang, X.; Zhan, J.; Wang, D. Solar Hydrogen Generation by  
32 Silicon Nanowires Modified with Platinum Nanoparticle Catalysts by Atomic Layer Deposition.  
33 *Angew. Chem. Int. Ed.* **2013**, *52*, 11119-11123.  
34  
35  
36  
37  
38 (21) Qiao, L.; Zhou, M.; Li, Y.; Zhang, A.; Deng, J.; Liao, M.; Xiao, P.; Zhang, Y.; Zhang, S.  
39 Enhancing Electrochemical Hydrogen Generation by Platinum-Modification of p-Type Silicon  
40 Wires Array under Visible Light. *J. Electrochem. Soc.* **2014**, *161*, H458-H463.  
41  
42  
43  
44  
45 (22) Oh, I.; Kye, J.; Hwang, S. Enhanced Photoelectrochemical Hydrogen Production from  
46 Silicon Nanowire Array Photocathode. *Nano Lett.* **2012**, *12*, 298-302.  
47  
48  
49  
50 (23) Ji, J.; Zhang, H.; Qiu, Y.; Wang, Y.; Luo, Y.; Hu, L. Platinum Nanoparticle Decorated  
51 Silicon Nanowire Arrays for Photoelectrochemical Hydrogen Production. *J. Mater. Sci. Mater.*  
52 *Electron.* **2013**, *24*, 4433-4438.  
53  
54  
55  
56 (24) Burda, C.; Chen, X.; Narayanan, R.; El-Sayed, M. A. Chemistry and Properties of  
57 Nanocrystals of Different Shapes. *Chem. Rev.* **2005**, *105*, 1025-1102.  
58  
59  
60

- 1  
2  
3  
4  
5  
6  
7  
8 (25) Somorjai, G. A. Surface Science and Catalysis. *Science* **1985**, 227, 902-908.  
9  
10 (26) Ahmadi, T. S.; Wang, Z. L.; Green, T. C.; Henglein, A.; El-Sayed, M. A. Shape-Controlled  
11 Synthesis of Colloidal Platinum Nanoparticles. *Science* **1996**, 272, 1924-1925.  
12  
13 (27) Ahmadi, T. S.; Wang, Z. L.; Green, T. C.; Henglein, A.; El-Sayed, M. A. "Cubic" Colloidal  
14 Platinum Nanoparticles. *Chem. Mater.* **1996**, 8, 1161-1163.  
15  
16 (28) Xia, Y.; Xiong, Y. J.; Skrabalak, S. E. Shape-Controlled Synthesis of Metal Nanocrystals:  
17 Simple Chemistry Meets Complex Physics ? *Angew. Chem., Int. Ed.* **2009**, 48, 60-103.  
18  
19 (29) Chen, J.; Lim, B.; Lee, E. P.; Xia, Y. Shape-Controlled Synthesis of Platinum Nanocrystals  
20 for Catalytic and Electrocatalytic Applications. *Nano Today* **2009**, 4, 81-95.  
21  
22 (30) Tao, A. R.; Habas, S.; Yang, P. Shape Control of Colloidal Metal Nanocrystals. *Small* **2008**,  
23 4, 310-325.  
24  
25 (31) Tian, N.; Zhou, Z.-Y.; Sun, S.-G.; Ding, Y.; Wang, Z. L. Synthesis of Tetrahedral  
26 Platinum Nanocrystals with High-Index Facets and High Electro-Oxidation Activity. *Science*  
27 **2007**, 316, 732-735.  
28  
29 (32) Tian, N.; Zhou, Z.-Y.; Sun, S.-G. Platinum Metal Catalysts of High-Index Surfaces: From  
30 Single-Crystal Planes to Electrochemically Shape-Controlled Nanoparticles. *J. Phys. Chem. C*  
31 **2008**, 112, 19801-19817.  
32  
33 (33) Huang, X.; Zhao, Z.; Fan, J.; Tan, Y.; Zheng, N. Amine-Assisted Synthesis of Concave  
34 Polyhedral Platinum Nanocrystals Having {411} High-Index Facets. *J. Am. Chem. Soc.* **2011**,  
35 133, 4718-4721.  
36  
37 (34) Narayanan, R.; El-Sayed, M. A. Changing Catalytic Activity during Colloidal Platinum  
38 Nanocatalysis Due to Shape Changes: Electron-Transfer Reaction. *J. Am. Chem. Soc.* **2004**, 126,  
39 7194-7195.  
40  
41  
42  
43  
44  
45  
46  
47  
48  
49  
50  
51  
52  
53  
54  
55  
56  
57  
58  
59  
60

- 1  
2  
3  
4  
5  
6  
7  
8 (35) Fu, X.; Wang, Y.; Wu, N.; Gui, L.; Tang, Y. Shape-Selective Preparation and Properties of  
9 Oxalate-Stabilized Pt Colloid. *Langmuir* **2002**, *18*, 4619-4624.  
10  
11 (36) Kinge, S.; Bonnemann, H. One-Pot Dual Size- and Shape Selective Synthesis of Tetrahedral  
12 Pt Nanoparticles. *Appl. Organomet. Chem.* **2006**, *20*, 784-787.  
13  
14 (37) Zhang, J.; Yao, W.; Liu, M.; Xu, Q.; Wu, Q.; Zeng, T. Shape Controlled Synthesis of  
15 Platinum Nanocrystals with High Catalytic Activities for Methanol Electrooxidation. *Catal. Lett.*  
16 **2013**, *143*, 1030-1034.  
17  
18 (38) Gong, H.; Sun, S.-G.; Chen, Y.-J.; Chen, S.-P. In Situ Microscope FTIRS Studies of CO  
19 Adsorption on an Individually Addressable Array of Nanostructured Pt Microelectrodes – An  
20 Approach of Combinatorial Analysis of Anomalous IR Properties. *J. Phys. Chem. B* **2004**, *108*,  
21 11575-11584.  
22  
23 (39) Wei, L.; Zhou, Z.-Y.; Chen, S.-P.; Xu, C.-D.; Su, D.; Schuster, M. E.; Sun, S.-G.  
24 Electrochemically Shape-Controlled Synthesis in Deep Eutectic Solvents: Triambic Icosahedral  
25 Platinum Nanocrystals with High-Index Facets and Their Enhanced Catalytic Activity. *Chem.*  
26 *Commun.* **2013**, *49*, 11152-11154.  
27  
28 (40) Li, Y.; Jiang, Y.; Chen, M.; Liao, H.; Huang, R.; Zhou, Z.; Tian, N.; Chen, S.; Sun S.  
29 Electrochemically Shape-Controlled Synthesis of Trapezohedral Platinum Nanocrystals with  
30 High Electrocatalytic Activity. *Chem. Commun.* **2012**, *48*, 9531-9533.  
31  
32 (41) Wei, L.; Fan, Y.-J.; Tian, N.; Zhou, Z.-Y.; Zhao, X.-Q.; Mao, B.-W.; Sun, S.-G.  
33 Electrochemically Shape-Controlled Synthesis in Deep Eutectic Solvents—A New Route to  
34 Prepare Pt Nanocrystals Enclosed by High-Index Facets with High Catalytic Activity. *J. Phys.*  
35 *Chem. C* **2012**, *116*, 2040-2044.  
36  
37  
38  
39  
40  
41  
42  
43  
44  
45  
46  
47  
48  
49  
50  
51  
52  
53  
54  
55  
56  
57  
58  
59  
60

- 
- 1  
2  
3  
4  
5  
6  
7  
8 (42) Carraro, C.; Maboudian, R.; Magagnin, L. Metallization and Nanostructuring of  
9 Semiconductor Surfaces by Galvanic Displacement Processes. *Surf. Sci. Rep.* **2007**, *62*, 499-525.  
10  
11  
12 (43) Zhang, X.; Qiao, Y.; Xu, L.; Buriak, J. M. Constructing Metal-Based Structures on  
13 Nanopatterned Etched Silicon. *ACS Nano* **2011**, *5*, 5015-5024.  
14  
15  
16  
17 (44) Quan, Z.; Wang, Y.; Fang, J. High-Index Faceted Noble Metal Nanocrystals. *Acc. Chem.*  
18  
19  
20  
21  
22 (45) Loget, G.; Padilha, J. C.; Martini, E. A.; de Souza, M. O.; de Souza, R. F. Efficiency and  
23  
24  
25  
26  
27  
28  
29  
30  
31  
32  
33  
34  
35  
36  
37  
38  
39  
40  
41  
42  
43  
44  
45  
46  
47  
48  
49  
50  
51  
52  
53  
54  
55  
56  
57  
58  
59  
60
- Stability of Transition Metal Electrocatalysts for the Hydrogen Evolution Reaction using Ionic  
Liquids as Electrolytes. *Int. J. Hydrogen Energy* **2009**, *34*, 84-90.